

## An Oceanic General Circulation Model (OGCM) investigation of the Red Sea circulation:

### 2. Three-dimensional circulation in the Red Sea

Sarantis S. Sofianos<sup>1</sup> and William E. Johns

RSMAS, University of Miami, Miami, Florida, USA

Received 17 October 2001; revised 13 May 2002; accepted 20 May 2002; published 8 March 2003.

[1] The three-dimensional circulation of the Red Sea is studied using a set of Miami Isopycnic Coordinate Ocean Model (MICOM) simulations. The model performance is tested against the few available observations in the basin and shows generally good agreement with the main observed features of the circulation. The main findings of this analysis include an intensification of the along-axis flow toward the coasts, with a transition from western intensified boundary flow in the south to eastern intensified flow in the north, and a series of strong seasonal or permanent eddy-like features. Model experiments conducted with different forcing fields (wind-stress forcing only, surface buoyancy forcing only, or both forcings combined) showed that the circulation produced by the buoyancy forcing is stronger overall and dominates the wind-driven part of the circulation. The main circulation pattern is related to the seasonal buoyancy flux (mostly due to the evaporation), which causes the density to increase northward in the basin and produces a northward surface pressure gradient associated with the downward sloping of the sea surface. The response of the eastern boundary to the associated mean cross-basin geostrophic current depends on the stratification and  $\beta$ -effect. In the northern part of the basin this results in an eastward intensification of the northward surface flow associated with the presence of Kelvin waves while in the south the traditional westward intensification due to Rossby waves takes place. The most prominent gyre circulation pattern occurs in the north where a permanent cyclonic gyre is present that is involved in the formation of Red Sea Outflow Water (RSOW). Beneath the surface boundary currents are similarly intensified southward undercurrents that carry the RSOW to the sill to flow out of the basin into the Indian Ocean. *INDEX TERMS:* 4243 Oceanography: General: Marginal and semiencllosed seas; 4255 Oceanography: General: Numerical modeling; 4532 Oceanography: Physical: General circulation; *KEYWORDS:* Red Sea, marginal sea, Oceanic General Circulation Model, water mass formation

**Citation:** Sofianos, S. S., and W. E. Johns, An Oceanic General Circulation Model (OGCM) investigation of the Red Sea circulation: 2. Three-dimensional circulation in the Red Sea, *J. Geophys. Res.*, 108(C3), 3066, doi:10.1029/2001JC001185, 2003.

### 1. Introduction

[2] The Red Sea is one of the most unexplored areas of the Northern Hemisphere oceans. Most of the available observations are sporadic and sparse in space making any attempt to construct a picture of the three-dimensional circulation in the Red Sea very difficult. The only exception is the area of the strait of Bab el Mandeb which has attracted the interest of several observational efforts during the past century [Vercelli, 1927; Siedler, 1968; Maillard and Soliman, 1984; Murray and Johns, 1997]. The circulation that emerges from these observations is a two-layer exchange flow of the inverse estuarine type that lasts from October to May, with a relatively fresh surface inflow and a deep outflow of the

very saline (39.7 psu) Red Sea Outflow Water (RSOW). This simple pattern is interrupted for 4 months, during the summer season (June to September), when a shallow surface outflow, a subsurface intrusion of Gulf of Aden Intermediate Water (GAIW), and a weaker deep RSOW outflow take place.

[3] North of the strait, inside the Red Sea, most of our knowledge of the circulation and distribution of oceanographic properties comes from a handful of expeditions that performed mostly hydrographic stations, and data sets from ships of opportunity which usually follow the central axis of the Red Sea. Based on this kind of data and the elongated shape of the basin, most of the descriptive and theoretical investigations of the Red Sea circulation follow a two-dimensional approach (in the latitude-depth plane). Between them, the most debated aspect is the relative importance of the thermohaline and wind forcing and their role in the circulation and stratification of the Red Sea. Because of the strong salinity gradient along the axis of the Red Sea and the

<sup>1</sup>Now at Department of Physics, University of Athens, Athens, Greece.

formation of the very saline outflowing water mass inside the basin, the buoyancy loss (mostly due to the large evaporation rate) has been thought by several investigators to be the basic controlling mechanism of the flow [Maury, 1855; Luksch, 1901; Neumann and McGill, 1962; Phillips, 1966; Tragou and Garrett, 1997]. Others believe that the wind-stress field is more important in determining the circulation pattern, while the thermohaline forcing plays a secondary role [Thompson, 1939a, 1939b; Siedler, 1969; Patzert, 1974a].

[4] Very few clear circulation features can be identified from the observations performed in the Red Sea. Vercelli [1927], during a winter expedition in the southern part of the basin, measured significant northward currents close to the coasts, especially the African coast. During a later cruise (winter 1929 [Vercelli, 1931]) in the central Red Sea, near Port Sudan, he observed a southward countercurrent at depths greater than 250 m in the open sea but less than 150 m near the coast. The area where the most consistent observations were undertaken is the northern part of the basin, north of 23 latitude. Two winter cruises (1935 on the R/V *MABAHISS* and 1963 on the R/V *CDT ROBERT GIRAUD*) acquired several hydrographic sections in the area [Morcos, 1970; Morcos and Soliman, 1974; Maillard, 1974]. The patterns of the estimated geostrophic currents agree in general, showing a cyclonic gyre at the extreme north which penetrates up to 300 m depth and an anticyclonic gyre about  $2^\circ$  to the south. The presence of the northern cyclonic eddy was later verified by a series of five drifter tracks during 1993–1994 which showed a consistent cyclonic circulation north of  $26^\circ\text{N}$  [Clifford *et al.*, 1997]. The temperature observations also support the presence of these features with colder waters at the center of the cyclonic flow and much warmer waters in the center of the anticyclonic flow. These characteristics can also be seen in later cruises [Quadfasel and Baunder, 1993] and can be attributed to vertical displacement of the isopycnals inside cyclonic and anticyclonic vortices. Thus the Red Sea appears to contain several quasipermanent gyres and intensified boundary currents and subsurface countercurrents that are only peripherally understood.

[5] In this study a general circulation ocean model, the Miami Isopycnic Coordinate Ocean Model (MICOM) [Bleck *et al.*, 1992; Bleck and Chassignet, 1994], is used to investigate the three-dimensional circulation in the Red Sea. In section 2 we provide a brief review of the atmospheric forcing over the Red Sea. In section 3 the model configuration and the forcing fields used will be discussed. Section 4 presents the results of the numerical simulation. In section 5, results from two additional experiments will be presented, investigating the different effects of the thermohaline and wind forcing. Finally, section 6 includes a summary and discussion of the overall picture of the Red Sea circulation emerging from this study.

## 2. Atmospheric Forcing

[6] The fresh water deficit of the Red Sea is one of the largest encountered in the world ocean, due to strong evaporation, very small precipitation and negligible river runoff. The actual  $E - P$  rate has been highly debated, and the values proposed by different investigators range from 1.5 to 2.3 m/year [Yegorov, 1950; Neumann, 1952; Privett,

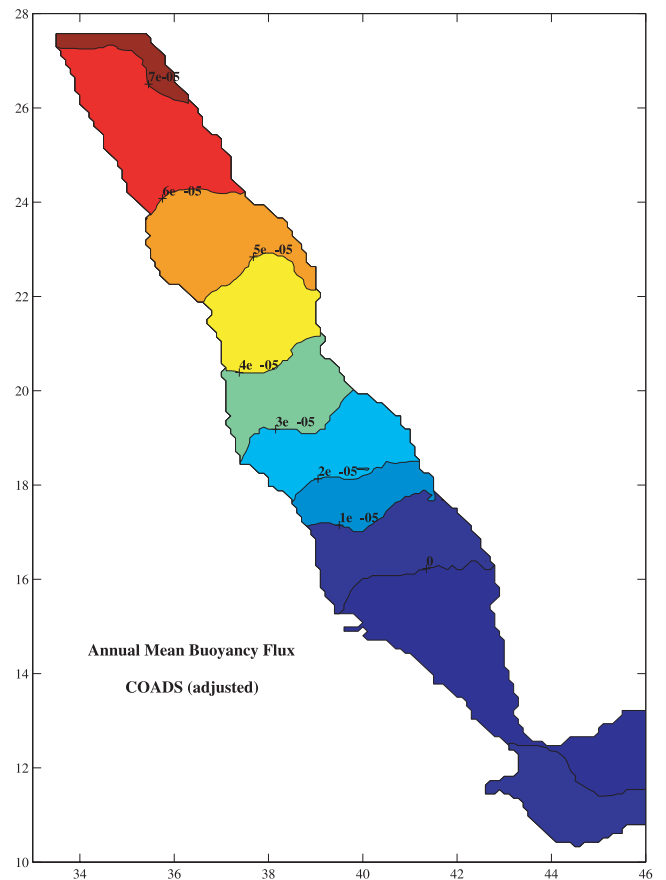


**Figure 1.** Annual mean distribution of the buoyancy flux over the Red Sea (in  $\text{kg m}^{-1} \text{s}^{-3}$ ), using the COADS climatology (adjusted to recent heat and freshwater fluxes estimates by Sofianos *et al.* [2002]).

1959; da Silva *et al.*, 1994; Tragou *et al.*, 1999]. Recent long-term observations at the strait of Bab el Mandeb [Murray and Johns, 1997] of the flow and the temperature/salinity characteristics of the water masses involved can be used to constrain the average freshwater budget of the whole basin. Using this data, the annual mean  $E - P$  rate is estimated at  $2.06 \pm 0.22$  m/year [Sofianos *et al.*, 2002]. Little is known about the temporal and spatial variability of the freshwater flux, and there are large discrepancies between available estimates [Yegorov, 1950; Neumann, 1952; Privett, 1959; da Silva *et al.*, 1994]. The latent heat flux associated with the  $E - P$  is very large (about  $160 \text{ W/m}^2$ ); however, the net radiative heat gain nearly balances this loss, so that the annual mean heat loss from the surface of the Red Sea is small,  $O(10 \text{ Wm}^{-2})$  [Patzert, 1974b; Tragou *et al.*, 1999; Sofianos *et al.*, 2002]. The combined effects of freshwater and heat flux add up to an annual mean buoyancy loss of approximately  $27 \times 10^{-6} \text{ kg m}^{-1} \text{ s}^{-3}$ . According to the Comprehensive Ocean-Atmosphere Data Set (COADS) [da Silva *et al.*, 1994], there is a significant seasonal cycle around this mean value with a large buoyancy loss during winter and a small buoyancy gain during summer, such that the total range of the annual cycle  $25 \times 10^{-6} \text{ kg m}^{-1} \text{ s}^{-3}$  is nearly equal to the mean value. A strong south to north mean gradient in the buoyancy forcing is also present in the basin (Figure 1).

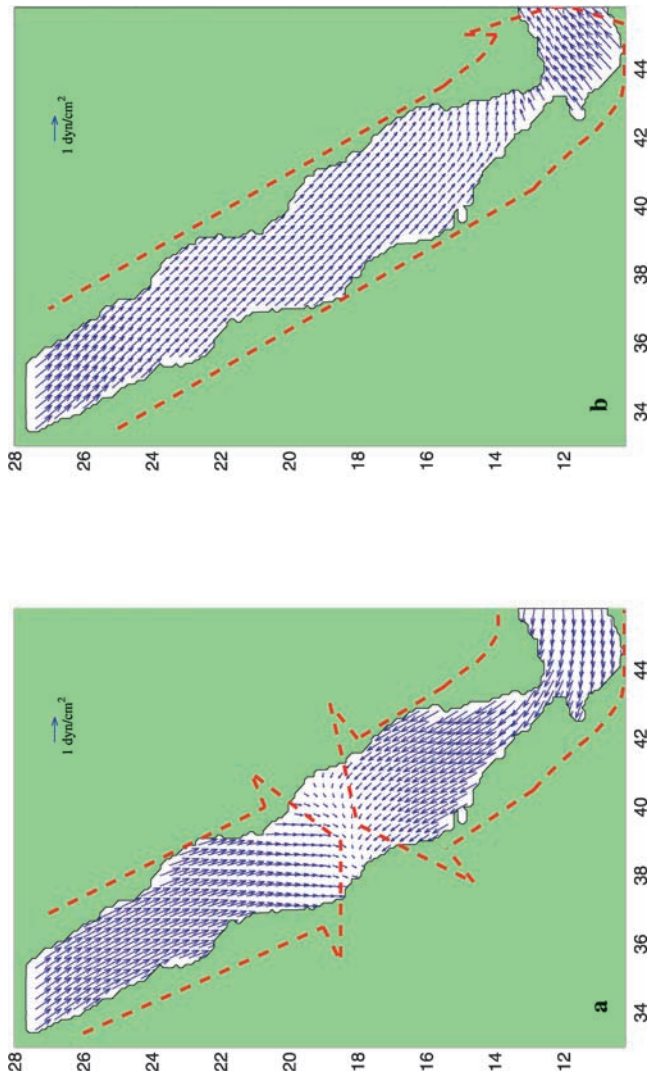


**Figure 2.** Wind-stress fields for (a) January and (b) July from COADS climatology.

[7] The Red Sea experiences strong and complicated wind forcing with surface winds that can reach speeds of more than 10 m/sec, intense land and sea breezes, and synoptic timescale variability. Since the focus of this paper is on the seasonal circulation patterns, the high-frequency variability will be neglected and the monthly mean wind fields will be used. Due to the existence of high mountain ranges along the African and Asian coasts, the direction of the surface winds is orographically steered along the axis of the Sea. The January and July mean fields of the wind-stress from COADS [da Silva et al., 1994] are plotted in Figure 2 and represent the winter and summer extremes. Two wind regimes are present, one in the northern part of the Red Sea and one in the southern part. The former is influenced by the eastern Mediterranean weather systems [Pedgley, 1974] and the wind is from the northwest all around the year. In the southern part of the basin the wind is controlled by the Indian Monsoon system, and it reverses from southeast during winter (October to May) to northwest during summer (June to September). Although this general pattern has been

well known for thousands of years and verified by many investigators, details of the wind field estimates differ between different data sets, especially in the northern part of the Red Sea. *The Koninklijk Nederlands Meteorologisch Instituut (KNMI)* [1949] atlas, utilized by Patzert [1974a], shows the strongest winds during summer in the northern part of the basin while in COADS the maximum winds occur during winter. Nevertheless, the basic seasonal cycle of the wind-stress is a very robust feature and combined with the intensity of the winds it makes the wind forcing an important mechanism for the Red Sea circulation.

### 3. Model

[8] MICOM is a primitive equation ocean model that has its vertical discretization in layers of constant potential density. An advantage of isopycnic coordinates is that the vertical resolution of the model can be intensified in regions of higher gradients and the presence of different water masses can be identified clearly over the full domain used in the simulation. This is very important in the case of the Red Sea which exhibits a complex exchange flow at the strait of Bab el Mandeb and a variety of water masses involved in the general circulation of the area.

[9] The vertical density structure is defined by six isopycnic layers and a variable-density mixed layer (Table 1). The choice of the number of layers and the  $\sigma_\theta$  of each layer was made in order to incorporate all the major water masses while keeping the model simple and computationally efficient. The distinction between water masses must take into account the temperature and salinity characteristics, since the density stratification does not always reflect the presence of a certain water type. It has been hypothesized that the core of the outflowing RSOW originates from intermediate depths in the Red Sea [Neumann and McGill, 1962; Cember, 1988; Sofianos, 2000] and so special attention was given to distinguish between deep and intermediate waters which possess similar temperature and salinity characteristics and differ only slightly in their density. The bottom layer represents the Red Sea Deep Water (RSDW) which fills the basin from about 200 m to the bottom. The layers above represent the intermediate layers involved in the Red Sea circulation, and the first isopycnic layer, just below the mixed layer, represents the core of the GAIW.

[10] The model domain includes the whole Red Sea basin and a part of the Gulf of Aden reaching to 45°E (Figure 3). At the open end of the domain at 45°E, a 0.5° wide buffer zone was fitted (Figure 3) where hydrography is relaxed toward monthly mean values derived from the *Levitus* [1982] climatology, with a relaxation time of 60 days. In the present simulations the grid interval was chosen at 0.1°

**Table 1.** Vertical Resolution (Layer Density) Used in the Model

Layer Number	Layer Density, $\text{kgm}^{-3}$	Description
1	mixed layer	surface layer
2	1025.75	core of the GAIW
3	1026.25	
4	1026.75	
5	1027.25	
6	1028.00	core of the RSOW
7	1028.60	RSDW

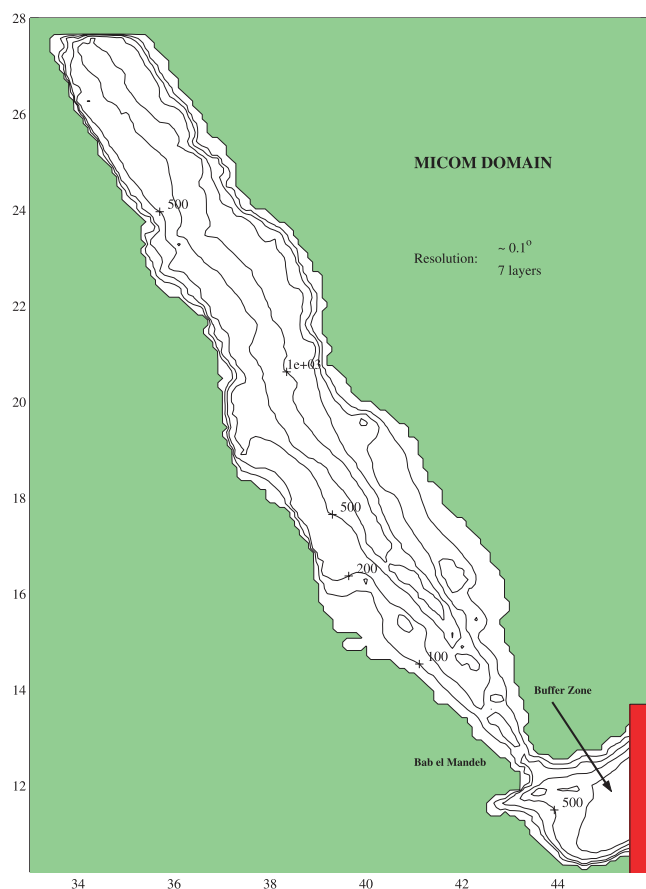


**Figure 3.** Domain and its bathymetry included in the OGCM experiments. The area indicated by red is the location of the buffer zone where hydrography is relaxed to Levitus climatology.

(or about 10 km) in order to resolve the exchange flow at the narrow strait. The two gulfs at the northern end of the Red Sea (Suez and Aqaba) are very small and were not included in the experiments performed. The wind and thermodynamic forcing applied to the model are derived from COADS [da Silva *et al.*, 1994] but with an additional  $0.5 \text{ m year}^{-1} E - P$  and  $60 \text{ W m}^{-2}$  of heat loss to the atmosphere for the reasons discussed by Sofianos and Johns [2002]. The model experiments were initialized using the National Oceanographic Data Center (NODC) hydrographic data for the winter state. For more discussion of the model, its configuration, and a description of the complete series of the experiments performed, the reader is referred to the work of Sofianos and Johns [2002].

[11] Three different model simulations are presented and discussed in this paper, which differ only in how they are forced. Both seasonal wind and seasonal thermohaline forcing are used for driving the model for the main experiment (E1). Two more experiments using only one of the two forcing mechanisms (thermohaline and wind) were carried out (E2 and E3, respectively). All the simulations were integrated for 10 years. Although the simulations did not reach absolute equilibrium after this time, the circulation develops very fast (within a few months) and does not change perceptibly after that either in its mean or seasonal

cycle. For all of the experiments, the results mentioned here are the average of the last 9 years of integration.

## 4. Results

[12] The performance of the model was tested at the strait of Bab el Mandeb where the resulting seasonal cycle of the exchange flow was compared with the available direct observations [Sofianos and Johns, 2002]. Although some differences in the phase and range of the two cycles exist, the main result is that the simulation is able to reproduce the basic characteristics of the observed variability. These features include the reversal of the surface flow in summer, the associated intermediate water intrusion, and the seasonal variability of the RSOW outflow with a minimum occurring during the summer. The strength of the annual mean exchange rate (0.38 Sv) is also nearly identical to the observed one (0.36 Sv). This increases our confidence in the results presented here, although comparison with future observations of the general circulation in the area will be a more definitive test.

### 4.1. Surface Circulation

[13] The 9-year average surface circulation for the winter (September to May) and summer (June to August) seasons are plotted in Figures 4 and 5, respectively. The

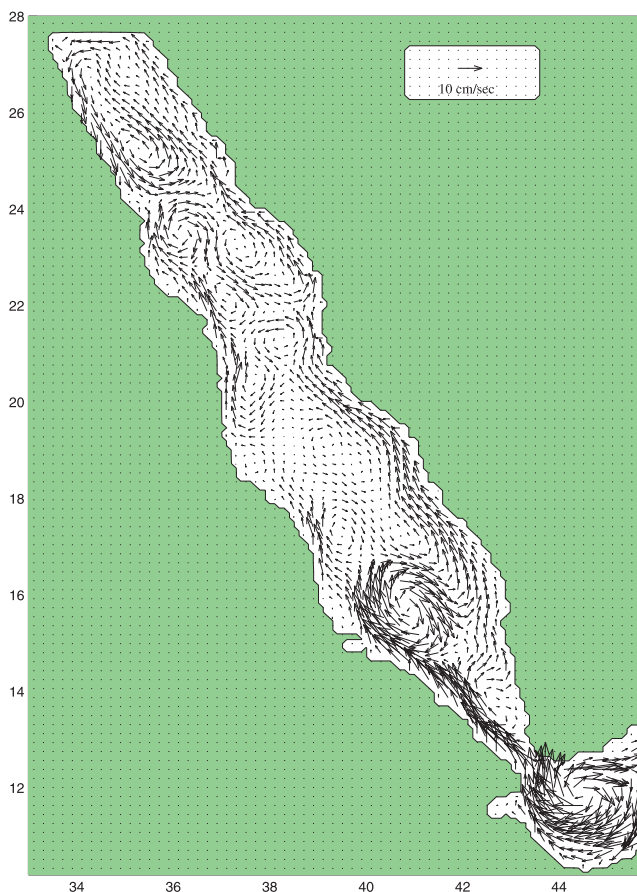


**Figure 4.** Mean winter surface circulation from MICOM simulation, using all forcing fields (experiment E1). The result represents the last 9 years of simulation.

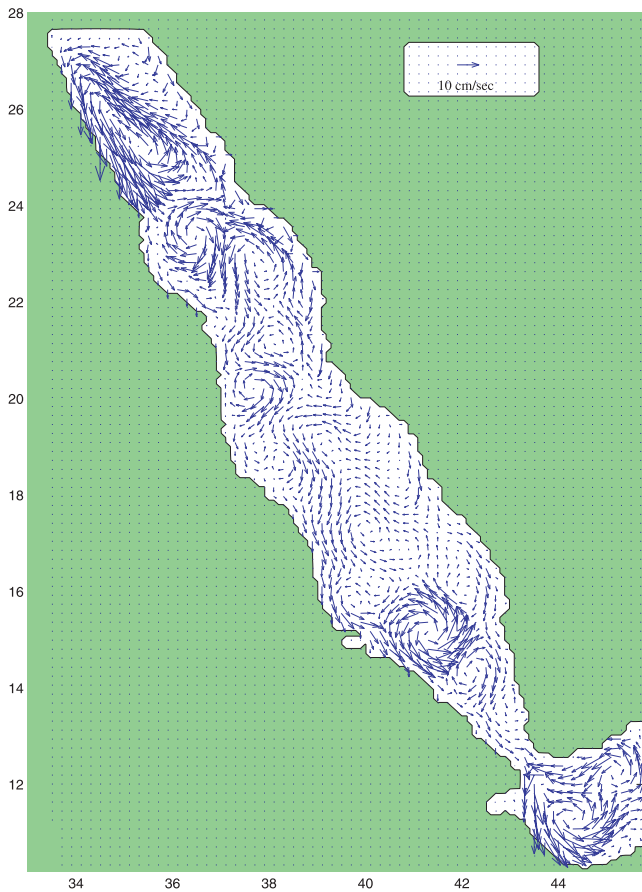


**Figure 5.** Mean summer surface circulation from MICOM simulation, using all forcing fields (experiment E1). The result represents the last 9 years of simulation.

choice of the months representing each season takes into account the seasonal patterns of the forcing fields as well as the exchange flow at the strait. Both wind and thermal forcing are highly variable at the seasonal time-scales, and thus the circulation patterns are expected to show a strong seasonality. All the fields show a high degree of complexity with a series of eddies and jet-like currents. Although the surface layer transport averaged across the basin is relatively weak (about 0.4 Sv and decreasing slowly to the north, in agreement with the order of magnitude predicted from the two-dimensional approaches), the cross-basin transport is very strong in accord with previous observations.

[14] South of 18°N the seasonal variability is strongest as expected by the reversal of the wind field as well as the high variability of the exchange flow at Bab el Mandeb. The dominant feature in the south is a mesoscale gyre with its center located between 15°N and 16°N which reverses from an anticyclonic rotation during winter to a cyclonic rotation during the summer and achieves velocities of more than 0.5 m/s during the peak of the winter. Other features present in the area are weaker and smaller, and most of them have a transient character.

[15] During winter, a strong surface inflow occurs at the strait. After entering the basin, this NNW flow intensifies along the western boundary as a strong boundary current

with maximum velocities that vary with the strength of the inflow but are greater than 20 cm/s throughout the season. After flowing only about 400 km into the Red Sea, near 16°N, this current ceases and an eastward intensified boundary current is observed for most of the remaining length of the basin. Although this boundary current is a little weaker and more variable than its southern counterpart, and it interacts with other features of the circulation (mesoscale cyclonic and anticyclonic eddies), it accounts for most of the surface northward flow in the basin.

[16] During summer the northward western boundary current disappears in the southern part of the Red Sea. It is during this season that the surface flow reverses and a strong intermediate inflow of the fresher and colder GAIW takes place. The model circulation now is relatively weaker and more irregular than in winter, since both wind and thermohaline forcing are weaker in summer.

[17] In the northern part of the Red Sea, two permanent eddies dominate the circulation field, a small anticyclonic gyre centered around 23.5°N and a larger, more elongated cyclonic gyre centered around 25°N. Both coincide surprisingly well with available observations in the region [Morcos, 1970; Morcos and Soliman, 1974; Maillard, 1974; Clifford *et al.*, 1997]. Although their strength, shape and extent show some seasonal variability, they are present throughout the year. The stronger one is the cyclonic gyre in the north reaching maximum velocities of more than 40 cm/s. This particular feature will be discussed in further detail later in association with intermediate water formation.

[18] The annual mean surface temperature and salinity fields are plotted in Figure 6. There is a distinct salinity gradient toward the north where it reaches its maximum, in agreement with the observations and simple theoretical models. The temperature pattern is more complicated, presenting its maximum at the center of the basin and decreasing toward the two ends of the Red Sea. This is related to the very weak wind speed observed in the central region of the Red Sea where the wind field is convergent for most of the year. These simple pictures are altered by the circulation complexity, and areas of minima and maxima are associated with the dominant features of the circulation pattern. A better idea of the temperature and salinity distribution and their association with the circulation and the atmospheric forcing is shown by the seasonal distribution of the two fields presented in Figures 7a–7d. During summer the surface temperatures become very warm with little meridional gradient over the basin, and therefore the annual mean pattern, with its maximum at midbasin, reflects mostly the winter pattern. However, it is very interesting to note the seasonal variability of zonal temperature gradient. During winter the highest temperatures are located at the eastern boundary (especially in the southern and central Red Sea), while during summer the eastern boundary is characterized by much lower temperatures (especially the northern and central Red Sea). This difference is associated with the prevailing winds which induce coastal upwelling along the eastern boundary in summer and downwelling in winter in the southern part of the basin. This effect is also reflected in the seasonal salinity distribution, where fresher surface waters are found along the eastern boundary in summer associated with upwelling of the cooler and fresher GAIW that is advected into the basin at this time of year.

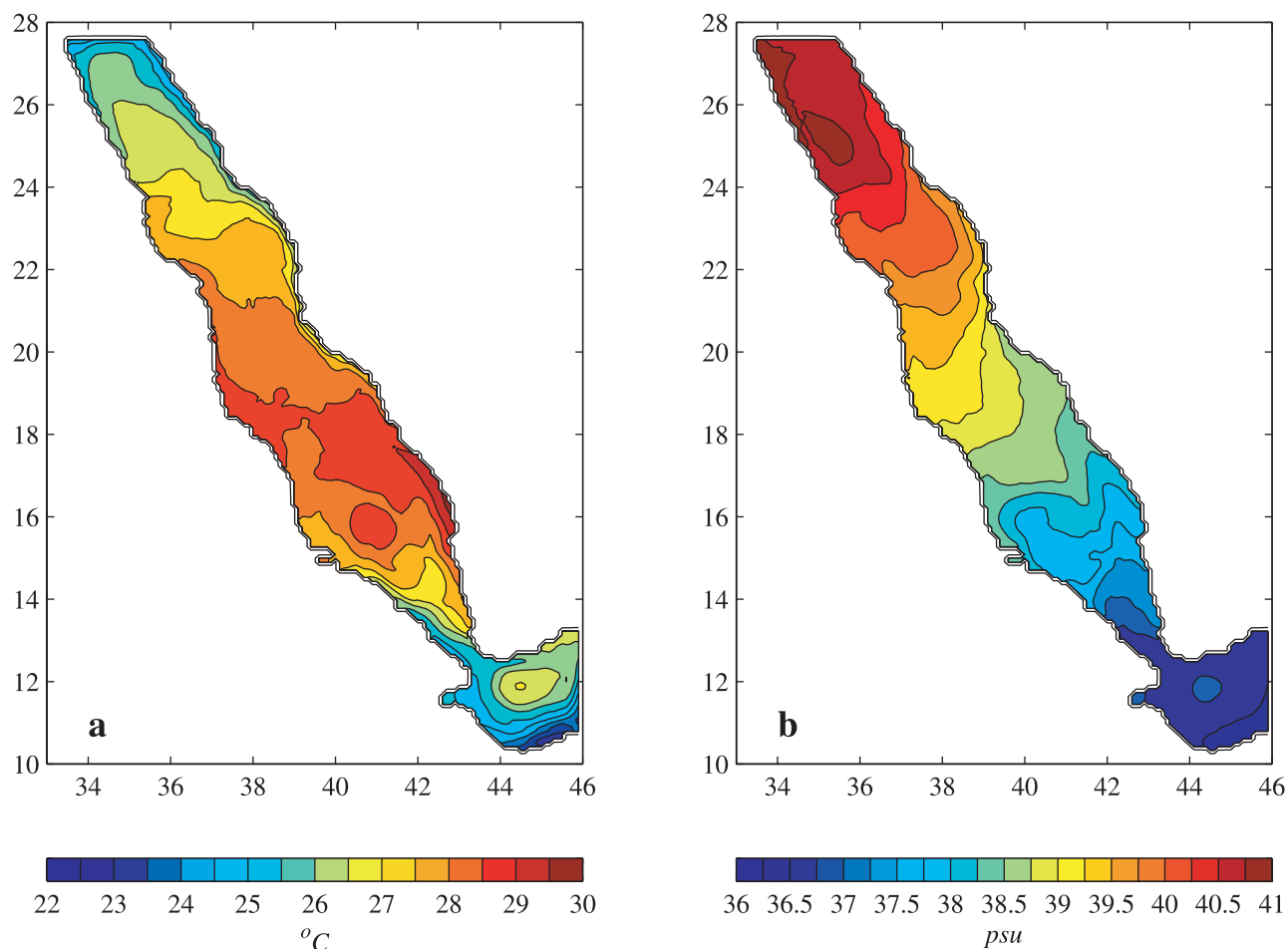


**Figure 6.** Annual mean (a) sea surface temperature and (b) salinity from MICOM simulation (experiment E1, average over the last 9 years of simulation).

[19] Figure 8 presents the 9-year average of the annual mean sea surface elevation anomaly. Apart from the highs and lows related to the circulation pattern, there is a downward tilt of the sea level to the north. Since the freshwater flux is imposed as a “virtual salinity flux” at the mixed layer, it cannot affect the volume of the basin, but will only increase the north-south density gradient, as evaporation is stronger in the northern part of the Red Sea. Thus the tilt is associated with the steric effect caused by the strong density gradient through the basin. An additional tilt is imposed by the static response to the southward winds, as discussed by *Sofianos and Johns* [2001].

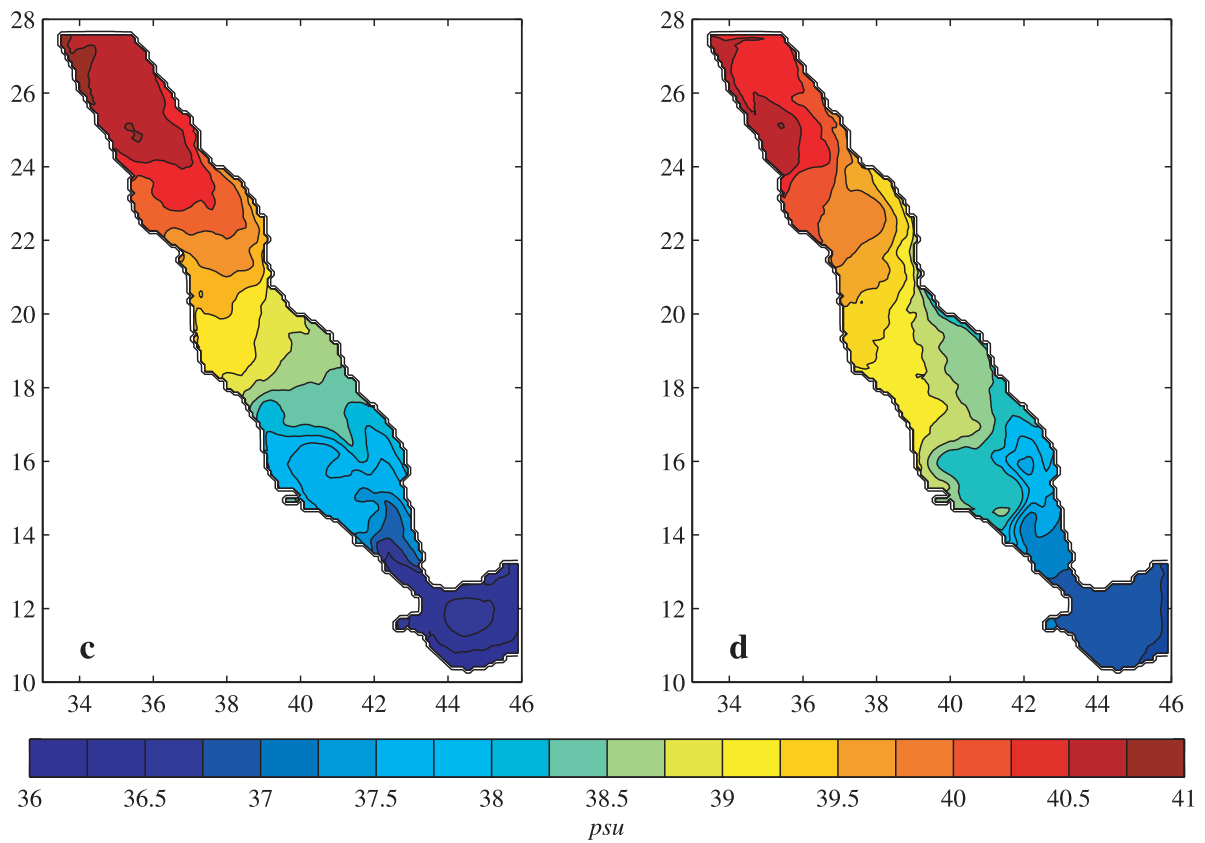
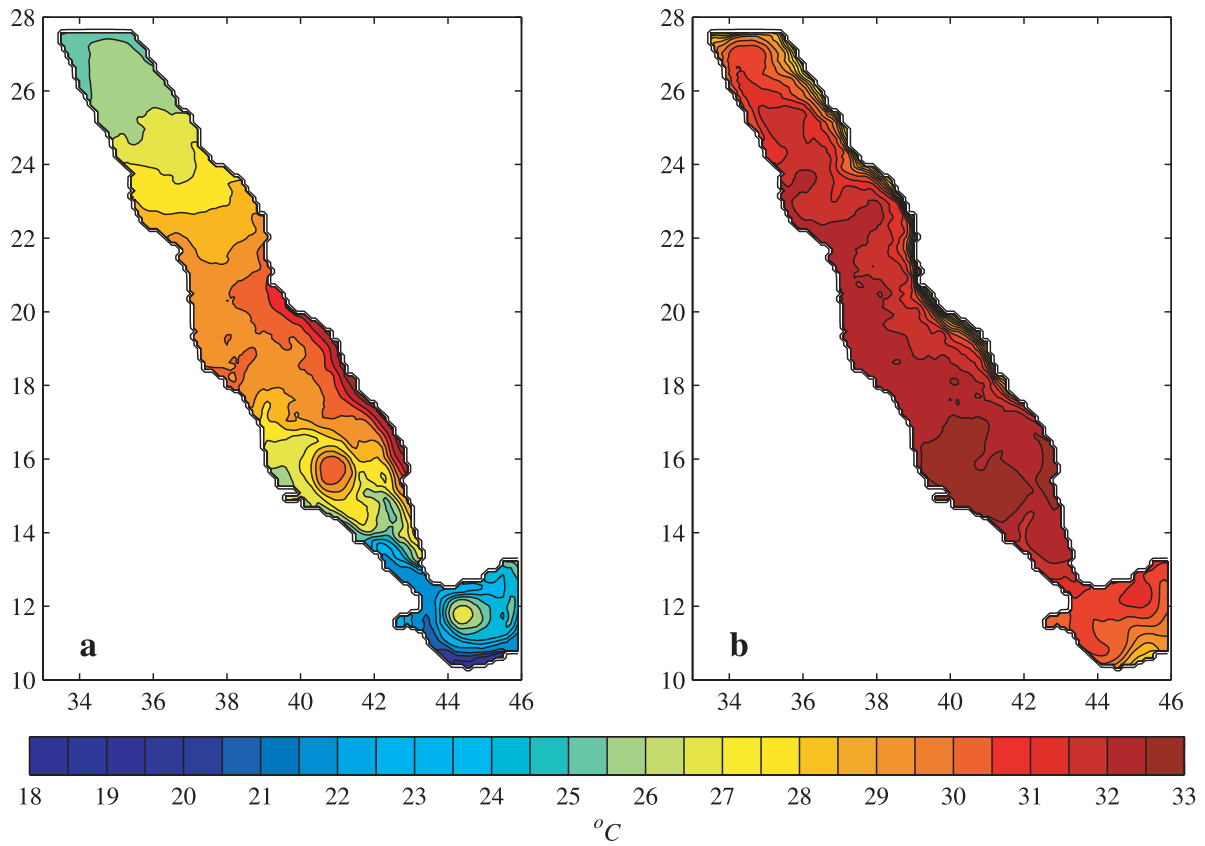
[20] The annual mean surface circulation and surface density are plotted in Figure 9 and will be compared with the results from two additional experiments described in section 5. Although this is an average of the 9 years of simulation, including both seasons, some of the most important features are present, such as the boundary currents, the anticyclonic eddy in the south and the double gyre system in the northern part of the basin. This happens because some of the features are permanent and also

because the winter season lasts about three fourths of the year and presents a more vigorous circulation than the summer one.

#### 4.2. Intermediate Circulation

[21] The most active subsurface layer is the second one from the bottom (layer 6), which overlies the RSDW layer that contains a very weak circulation. Layer 6 is the core of the RSOW where most of the hypersaline outflow (39.8 psu from the model results compared to 39.7 psu from observations [*Murray and Johns*, 1997]) takes place at the bottom of the strait of Bab el Mandeb. The winter and summer circulations in this layer are plotted in Figures 10 and 11. The velocity field is weaker than the surface but involves several interesting features. It is also much less seasonally variable than the surface layer. The overall flow is southward, and its magnitude increases to the south near the Bab el Mandeb due to topographic constrictions and because of entrainment from the adjacent layers. It is obvious that the main surface circulation features directly affect the flow at this intermediate level, such as the the strong gyres in the

**Figure 7.** (opposite) Seasonal sea surface temperature and salinity distribution. (a) Winter (November–March) and (b) summer (June–September) sea surface temperature. (c) Winter and (d) summer sea surface salinity (experiment E1, average over the last 9 years of simulation).



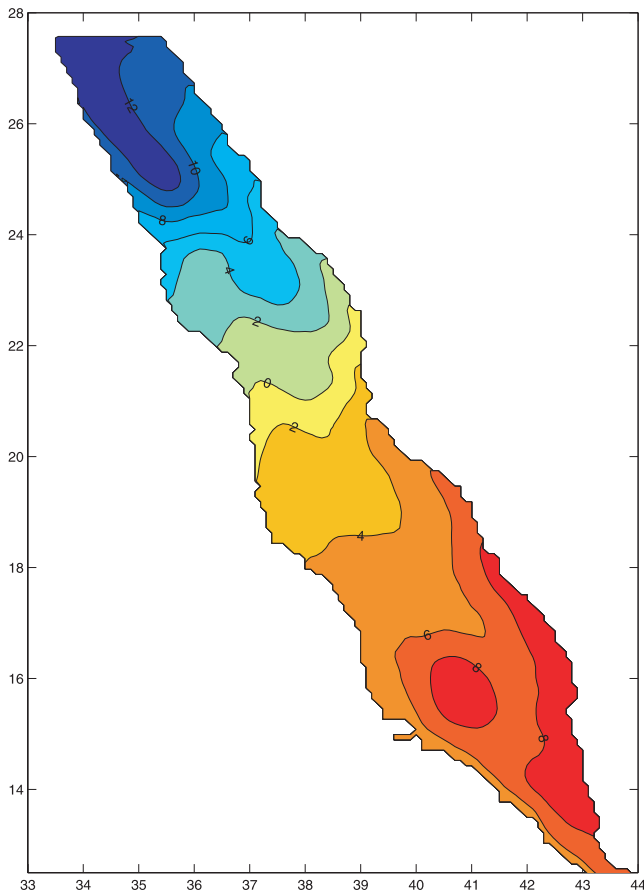


**Figure 8.** Annual mean sea surface elevation anomaly (in centimeters) from MICOM simulation (experiment E1, average over the last 9 years of simulation).

north which extend to the depth of layer 6. Boundary intensification is also observed in this layer, especially south of 20°N. The general pattern of this intensification has the characteristics of an undercurrent (i.e., opposite to the surface boundary currents), but the transition point is shifted to the north and the currents are affected by topography. Reaching the strait, the velocities in this layer become very large, achieving values of over 0.5 m/s.

[22] It should be noted that the magnitude of the intermediate depth circulation in summer may be overestimated by the model because the outflow of RSOW in the model, while smaller in summer, does not decrease to the very low values seen in observations [see *Sofianos and Johns, 2002*]. One would therefore expect the intermediate undercurrents to be considerably weaker in summer, since they are the primary conduits for transporting the RSOW water to the southern Red Sea and the Bab el Mandeb strait. The overall seasonality of the intermediate depth circulation may thus be larger than predicted by the model. A related consequence is that the compensating inflow of GAIW in the overlying layers in summer may be too large.

#### 4.3. Formation of the Red Sea Outflow Water

[23] The location, time and mechanisms involved in the formation of the RSOW inside the Red Sea basin are not yet clear. Until recently the outflowing water mass was confused with the RSDW. Most investigators agree that the

RSDW is formed during winter in the Gulf of Suez [*Maillard, 1974; Wyrki, 1974*] where that water obtains extreme values of salinity and sinks to the bottom of the Red Sea basin entraining ambient water. The Gulf of Aqaba is thought to be a secondary source of RSDW [*Wyrki, 1974*]. Other modes of formation have been hypothesized, such as open ocean deep convection and formation on the continental shelf of the Red Sea, but there is no evidence to support them. The idea that the outflow originates from intermediate depths was proposed by *Neumann and McGill [1962]*. Analyzing tracer distributions ( $^{14}\text{C}$  and  $^3\text{He}$ ) from the GEOSECS Indian Ocean Expedition, *Cember [1988]* was the first to clearly identify a different water mass comprising the core of the outflow (which he called RSOW to distinguish it from the RSDW). Further evidence in support of this hypothesis is the small rate of RSDW formation. The only direct observation of the transport at the mouth of the Gulf of Suez during the winter is that of *Maillard [1974]* during 1971–1972 which gives an estimated deep water outflow of 0.082 Sv, or, assuming that this is representative of 3 winter months, an annual rate of approximately 0.02 Sv. *Maillard [1974]* assumed that this transport is doubled due to entrainment, so that the total RSDW production is  $O(0.04 \text{ Sv})$ . This is a very small amount compared to the total outflow from the Red Sea

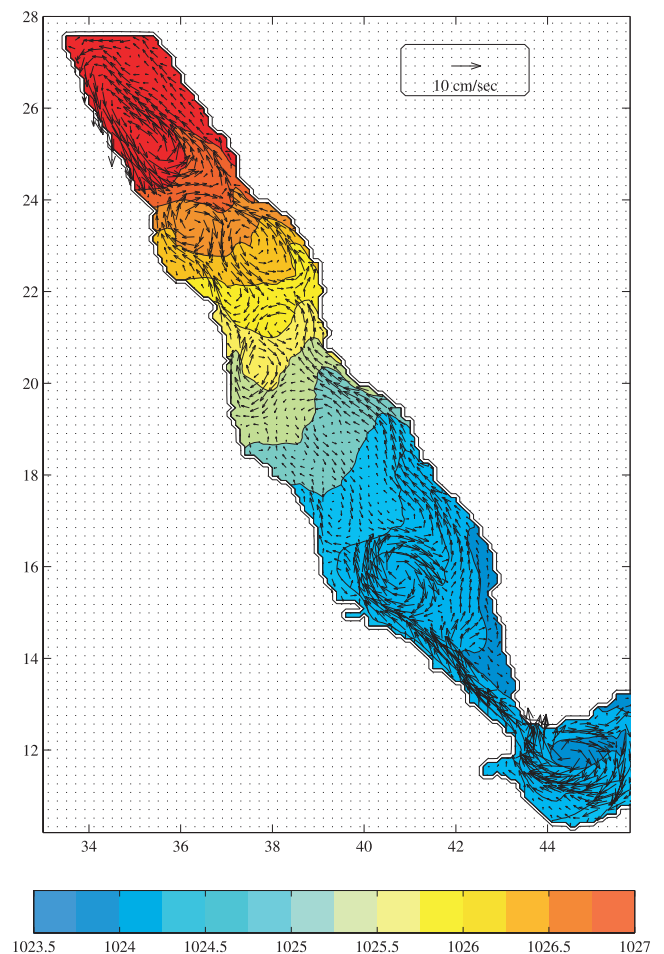


**Figure 9.** Annual mean surface circulation superimposed on the mixed layer density from the full-forcing MICOM simulation (9-year average).

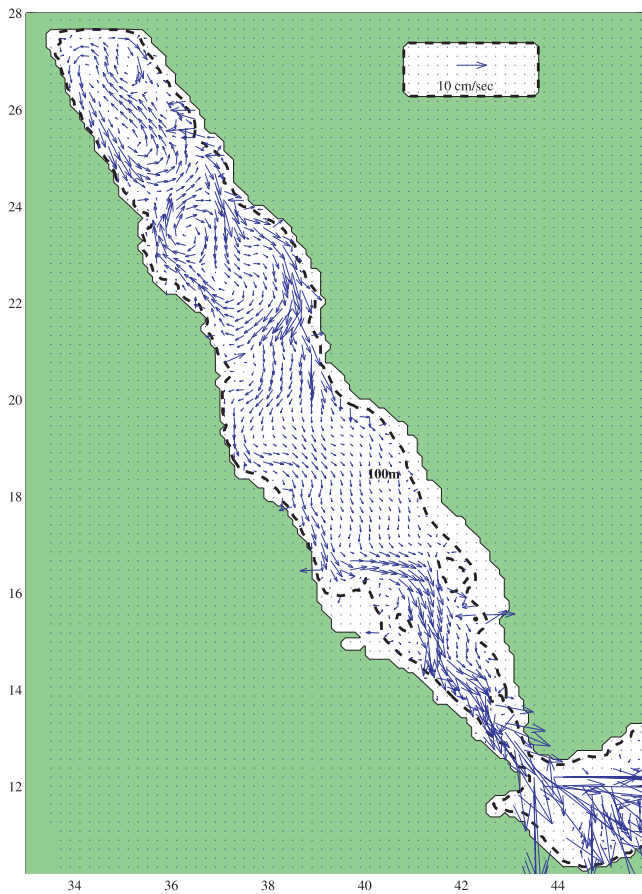


**Figure 10.** Mean winter layer 6 circulation from MICOM simulation, using all the forcing fields (experiment E1). The result represents the last 9 years of simulation.

which is an order of magnitude larger. Recent observations in the Red Sea [Woelk and Quadfasel, 1996] of the oxygen distribution verify the distinction between the deep and intermediate waters. An oxygen minimum at intermediate depths (about 300 m) separates a relatively new intermediate water mass (the RSOW) from much older deep water (RSDW).

[24] Cember [1988] proposed that this intermediate water mass is injected immediately beneath the pycnocline at a rate of  $0.11 \pm 0.02\text{Sv}$ , and located the place of formation at the extreme northern open Red Sea. Unfortunately, no direct observations are available to verify this hypothesis, and due to insufficient data, very little can be said about the mechanisms involved in this formation process.

[25] Since the strength and properties of the exchange flow at Bab el Mandeb are reasonably well reproduced by the model [Sofianos and Johns, 2002], its results may be used to investigate mechanisms involved in the RSOW formation, possible locations, and rates of production. The most likely area for RSOW formation is the northern Red Sea, since the strongest buoyancy forcing takes place there (Figure 1). Localized open ocean deep and intermediate convection is one of the most important mechanisms of water mass formation in the oceans and is present in many polar or low-latitude semienlosed basins such as the western Mediterranean [Swallow and Caston, 1973; Leaman and Schott, 1991], the eastern Mediterranean [Lascazatos,

1993], the Labrador Sea [Clarke and Gascard, 1983], the Greenland Sea [Schott et al., 1993; Visbeck et al., 1995] and Weddell Sea [Gordon, 1978; Muench, 1988; Alverson and Owens, 1996]. Although localized buoyancy loss can be important in these features, the typical atmospheric scale of forcing is an order of magnitude larger than the observed structures. Furthermore, vertical stratification and the Coriolis force act together against convective motions. In order for deep or intermediate convection to take place, two more conditions must also contribute: weak stratification and a “trapping mechanism” to keep the surface waters exposed to strong atmospheric forcing for enough time to acquire the proper temperature and salinity characteristics. These elements are known as the preconditioning phase [Swallow and Caston, 1973; Hogg, 1973] which can result from a variety of mechanisms. In most of the known cases, this preconditioning is associated with a cyclonic gyre where the stratification weakens due to upward tilt of the isopycnals, and waters are exposed for a considerable time to intense buoyancy loss. In the eastern Mediterranean, where the atmospheric conditions resemble those of the northern Red Sea (i.e., extensive evaporation), the formation of the Levantine Intermediate Water is a localized winter process in the region of the Rhodes Gyre in the Levantine basin [Lascazatos et al., 1993]. The depth to which the convective plumes penetrate depends on the vertical stratification and the time and intensity of the buoyancy flux.

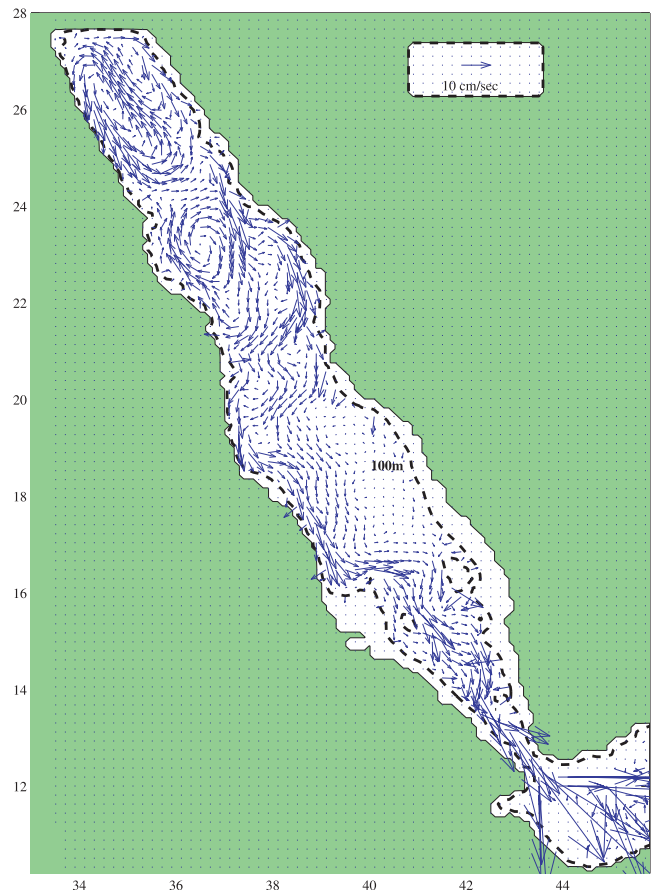


**Figure 11.** Mean summer layer 6 circulation from MICOM simulation, using all the forcing fields (experiment E1). The result represents the last 9 years of simulation.

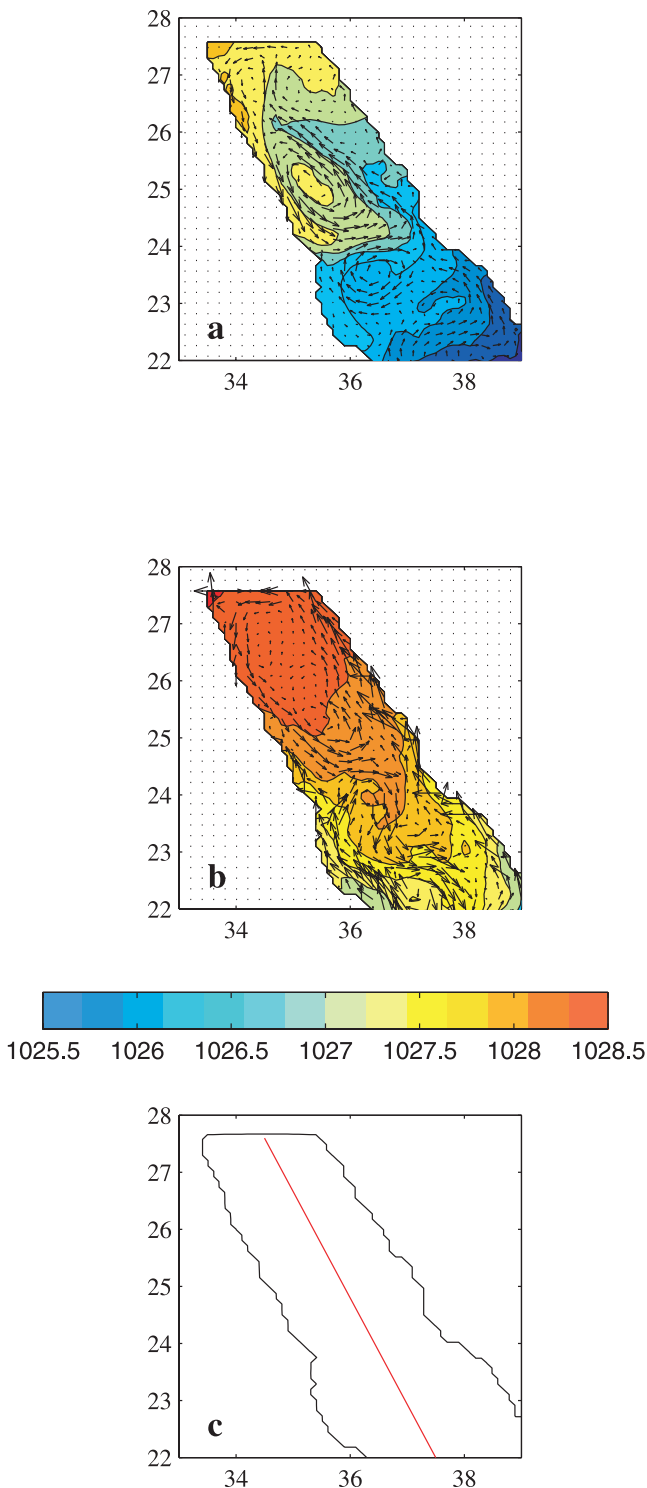


**Figure 12.** Mean surface velocity and density from the MICOM simulation at the northern Red Sea for (a) November and (b) February. (c) Location of the vertical section presented in Figure 13 is indicated by the red line.

[26] The results of the model simulation suggest that a similar process is involved in the RSOW formation in the northern Red Sea. In Figure 12 the density and velocity of the surface layer is plotted for different months representing the “preconditioning” and actual formation periods. As

noted before, the most significant circulation feature is the permanent cyclonic gyre centered at about  $25^{\circ}\text{N}$ . Inside this gyre the mixed layer achieves high densities throughout the year, and at the peak of the winter season the mixed layer has density close to the RSOW layer. The “trapping ability” of this gyre is also evident from the density patterns. The mixed layer density and underlying layer thicknesses along a transect through the northern Red Sea for November, February, and April, averaged over the last 9 years of simulation, are presented in Figure 13. These months coincide with the preconditioning phase, the period when the strongest intermediate water formation takes place, and the period when the mixed layer retreats due to buoyancy addition from the surface fluxes. The higher densities near  $25^{\circ}\text{N}$  (Figure 13a) is clear evidence of weaker stratification inside the gyre, enabling a more efficient homogenization of the upper water column. During February (Figure 13b) the mixed layer is very deep (reaching 300 m depth at the northern end of the basin) and penetrates up to the sixth

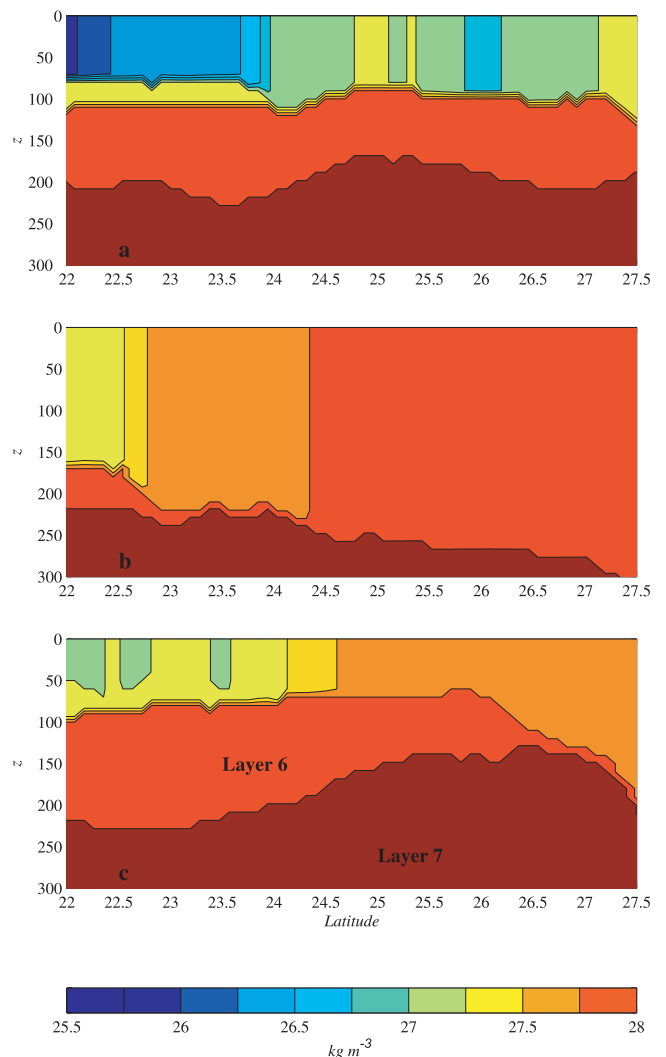


**Figure 13.** Vertical stratification along a section following the central axis of the northern Red Sea for (a) November, (b) February, and (c) April, representing the sequence of “preconditioning,” formation, and retreat of the mixed layer phases, respectively.

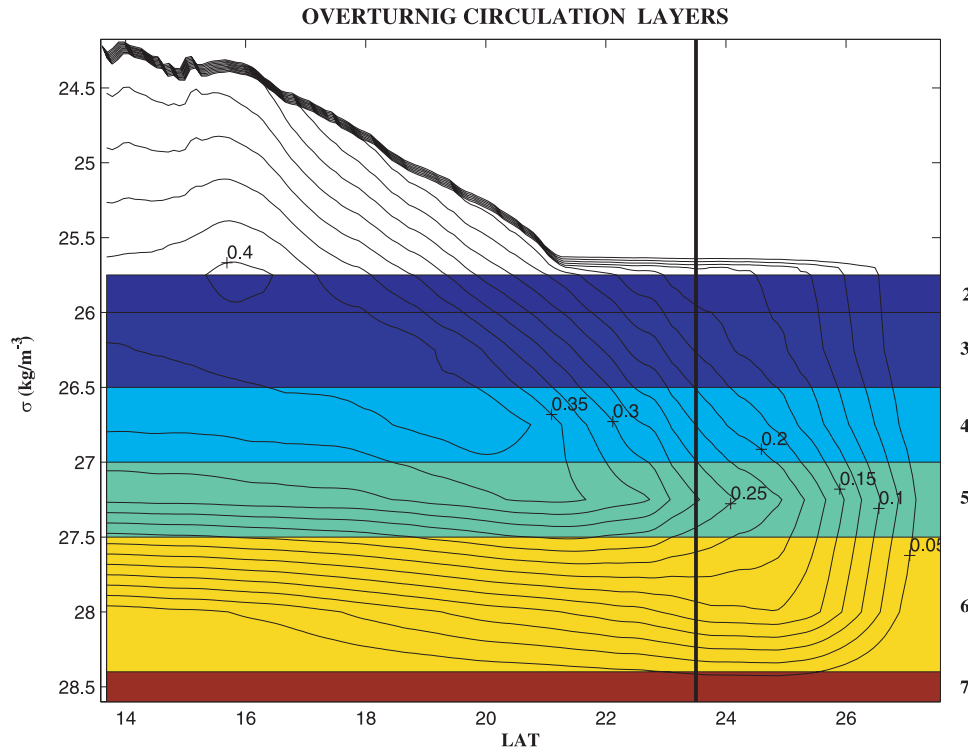


**Figure 14.** Mean overturning circulation from the MICOM simulation. The thick vertical line shows the southernmost annual limit of the northern cyclonic gyre where most of the RSOW is formed.

layer (the layer which corresponds to the core of the RSOW). The sixth layer disappears north of about 24°N. This is the actual formation period, when the RSOW is replenished through open ocean convection. Following the formation phase, the mixed layer retreats quickly and the stratification is reestablished, as shown in the April transect (Figure 13c). The sixth layer reinflates progressively, filled with the newly formed RSOW. Also seen in Figure 13 is the raising of the interface at the top of the RSDW in the northern part of the basin as the RSOW is evacuated from the basin, which is a large-scale baroclinic adjustment to the meridional pressure gradient.

[27] In order to get a more quantitative estimation of the amount of RSOW produced in the area of the cyclonic gyre, the mean overturning circulation on a  $\sigma\theta$ -latitude plane is plotted in Figure 14. Since this is an average over all the months and the 9 years of simulation, it is a smooth representation of the mass fluxes inside the basin. The lowest latitude that the southern edge of the cyclonic gyre reaches during the year is 23.5°N. The total formation of RSOW north of this latitude is about 0.25Sv or about 65% of the RSOW outflow. The remainder is formed north of 20°N latitude by entrainment into the RSOW layers. Thus it can be concluded that the dominant formation region for the RSOW is the northern Red Sea where the cyclonic gyre and strong buoyancy forcing in winter provide a favorable environment for intermediate depth convection.

## 5. Thermohaline- and Wind-Driven Experiments

[28] Although the effects of the wind stress and the thermohaline forcing do not combine linearly to drive the general circulation, it is sometimes convenient to separate

them and investigate the circulation produced by each one (what are usually called the wind- and thermohaline-driven parts of the circulation). Mechanistically these forcings interact through the effect of wind speed on the air-sea buoyancy fluxes and stirring of the mixed layer, and dynamically they interact to produce the final circulation and stratification patterns. With the above caveats in mind, two experiments with the same configuration, described in section 3, were carried out (E2 and E3), but with one forcing field “turned off,” wind and thermohaline, respectively. The main goals of these additional experiments are twofold: to estimate the relative strength and importance of each mechanism in the general circulation and, if possible, to determine the role each one plays in driving the key features of the circulation pattern presented in section 4.

[29] The annual mean surface velocity fields for the thermohaline- and the wind-driven cases are plotted in Figures 15 and 16, respectively (and can be compared with Figure 9 of the full forcing experiment). It is obvious from a comparison between the two results that the purely wind-driven circulation is much weaker than the thermohaline-driven one. This is not a result of the annual averaging, but persists throughout the year. Another indication that the thermohaline forcing is the dominant forcing mechanism is that in the areas where these two mechanisms compete with each other the patterns generated by the thermohaline forcing are the ones that prevail. This is the case in the northern end of the Red Sea, where the wind-driven circulation is anticyclonic while the thermohaline forcing drives a strong cyclonic eddy, which is a permanent feature of the circulation in the area as shown in section 4 and verified by observations. In areas where the two results have similar features (as in the case of of the winter anticyclonic

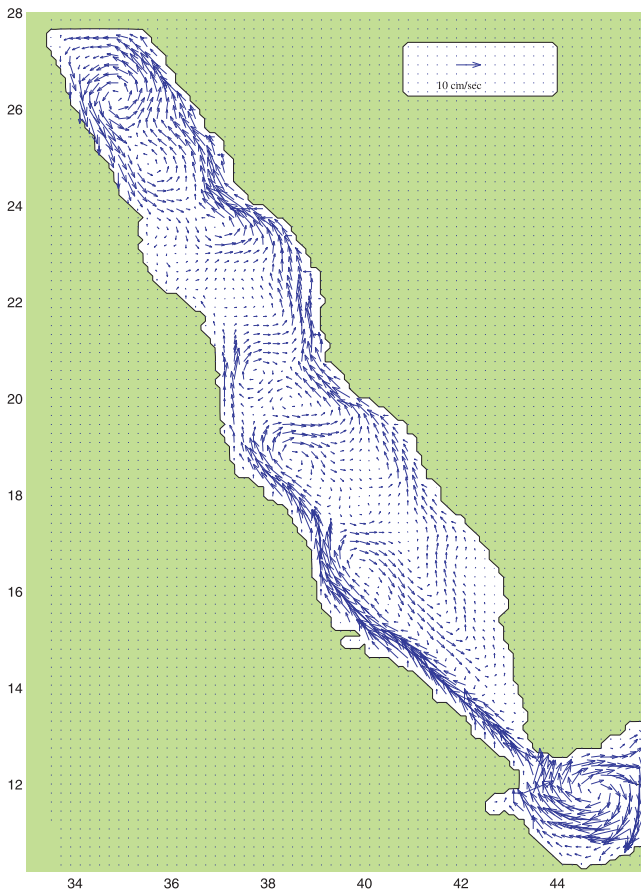


**Figure 15.** Nine-year average sea surface velocity from the MICOM experiment driven by the thermohaline fields only (E2).

eddy around 16°N), they reinforce each other, producing stronger circulation patterns. In a very few locations, there are features of the circulation that appear to be specifically linked to the winds; for example, the western boundary flow that is present in the combined forcing experiment near 22°N is present only in the wind-driven experiment. However, it is clear that the general circulation pattern of the combined forcing experiment mostly follows that of the thermohaline forced experiment.

[30] It is very interesting to notice that the thermohaline-driven result presents a similar type of intensification toward the coasts as seen in the combined forcing experiment (E1), with boundary currents shifting from the west to east coasts at midbasin, though shifted to the north by a few degrees relative to E1. This vigorous and complicated pattern of the thermohaline circulation is in sharp contrast to previous studies [Phillips, 1966; Tragou and Garrett, 1997] that predict a sluggish and two-dimensional type of circulation. Theoretical investigation can help give some insight into the possible mechanisms involved in these patterns. A relevant study is that by McCreary *et al.* [1986], who investigated the effect of thermohaline forcing on the setup of eastern boundary currents. If the density increases poleward, as is the case in the Red Sea, the resulting surface elevation field slopes downward in the same direction, creating an eastward geostrophic current in

the basin. This will affect the eastern boundary where downwelling must take place. McCreary *et al.* incorporated this idea into a three-dimensional, linear, continuous stratified theoretical model and solved for both steady thermodynamic forcing and forcing that oscillates in time with frequency  $\sigma$ . For the inviscid case, the solution at the eastern boundary will involve waves that are described by the dispersion relation

$$k = -\frac{\beta}{2\sigma} \left[ 1 - \left( 1 - 4 \frac{\sigma^2 \alpha^2}{\beta^2} \right)^{1/2} \right] \quad (1)$$

where  $k$  is the zonal wavenumber,  $\sigma$  is the forcing frequency,  $\alpha_{\eta}^{-1} = c_{\eta}/2 \Omega \sin(\theta)$  is the Rossby radius of deformation of the  $\eta$ th normal mode (with speed  $c_{\eta}$ ) and  $\beta = 2 \Omega \cos(\theta)/R$  is the meridional change of the Coriolis parameter, where  $R$  is the Earth's radius. The radicand vanishes at a latitude, the critical latitude  $\theta_{cr}$ , given by

$$\theta_{cr} = \tan^{-1}(c_{\eta}/2R\sigma). \quad (2)$$

North of  $\theta_{cr}$ ,  $k$  is complex, representing Kelvin waves that decay offshore rapidly with an  $e$ -folding scale of the order of  $\alpha^{-1}$ . South of the critical latitude,  $k$  is real and the waves that are generated are Rossby waves that propagate

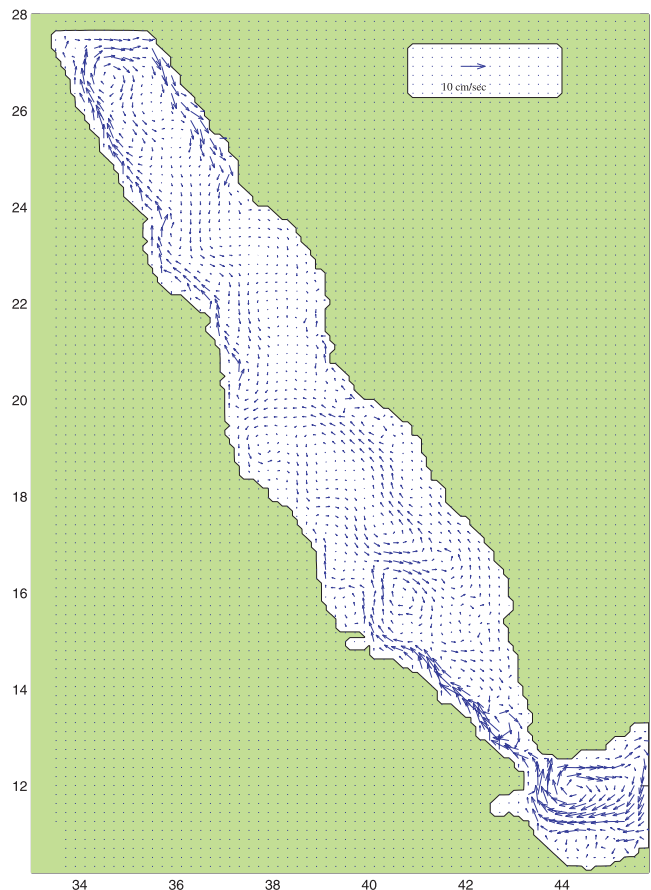


**Figure 16.** Nine-year average sea surface velocity from the MICOM experiment driven by the wind-stress fields only (E3).

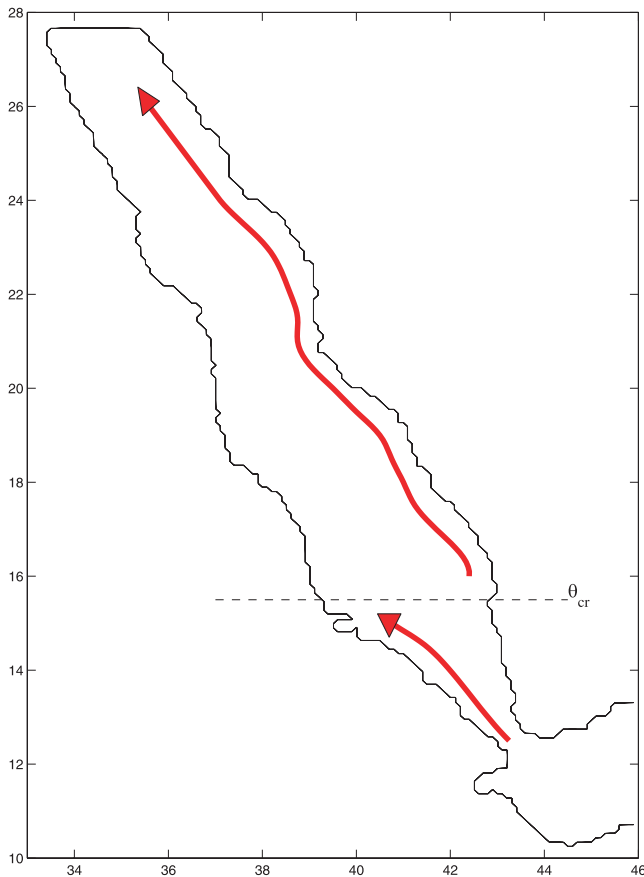


**Figure 17.** Schematic presentation of the flow intensification toward the coasts.

offshore (westward). So, we expect a westward intensification of the meridional flow south of  $\theta_{cr}$  as Rossby waves propagate the pressure gradient to the western boundary, and eastward intensification north of  $\theta_{cr}$ , as indicated in the schematic of Figure 17. The essential physics of this process is that Rossby waves are prevented from adjusting the basin to western intensified flow where their group velocity (at a specific frequency) is less than the eastward advection caused by the meridional density gradient. Since for fixed stratification this group velocity depends only on the latitude (decreasing to the north), a critical latitude can be established in the basin for certain model parameters.

[31] Direct application of the above formulas to the model results is difficult, since the stratification and the thermohaline forcing vary in space and time and cannot be compared with the idealized functions used in the theoretical model. Nevertheless, using the annual frequency and the basinwide mean stratification from the thermohaline-driven experiment results, the critical latitude is estimated at about  $17^\circ\text{N}$  (for the second baroclinic mode which is dominant in the Red Sea circulation, presenting a two-layer flow on the top of a mostly inactive layer, as confirmed by vertical EOF mode calculations). The addition of the wind does not significantly change the circulation pattern but is able to change the stratification enough to shift the critical latitude to the south. Using the mean stratification from the main experiment (with both forcing

fields), the new critical latitude is estimated at about  $14.5^\circ\text{N}$ , which is consistent with the southward shift of the boundary current transition in the experiment E1 compared to the thermohaline-only experiment (E2). While it is pointless to press the details of this comparison, these results strongly suggest that the meridional surface density gradient in the Red Sea is the main factor responsible for the transition of the boundary current system from the western to the eastern boundary at midbasin. This switch of the boundary current system is an interesting and robust feature of the circulation pattern in the model that awaits verification by observations.

## 6. Summary and Discussion

[32] The numerical simulation study of the Red Sea presented here suggests several interesting features of the circulation in the area. The most important findings include the intensification of the flow toward the coasts, the presence of the permanent double gyre system in the northern part of the basin, and the stronger seasonality of the flow in the southern part of the basin. A particularly interesting finding is the transition from western to eastern intensified boundary current regions between the southern and northern parts of the basin predicted by the model. As more observations become available and modeling efforts become more sophisticated, ideas about the circulation in the Red Sea are changing rapidly. The picture of a sluggish circulation proposed by the simplified two-dimensional approaches seems inadequate to describe the Red Sea dynamics. The patterns of the circulation are vigorous and complicated. These differences will have an important effect on the mixing processes and may answer some puzzling questions concerning the large-scale dynamical balances and net dissipation rates in the basin [Tragou and Garrett, 1997; Sofianos, 2000].

[33] Overall, the thermohaline forcing seems to be the most important mechanism driving this highly complex circulation. The main circulation pattern is related to the buoyancy loss (mostly due to evaporation) which increases the density to the north and produces a northward pressure gradient associated with the sloping of the sea surface. An eastward mean cross-basin geostrophic current is established in the upper layer. The response of the eastern boundary depends on the stratification and  $\beta$ -effect, and two different regimes were identified. North of a critical latitude an eastward intensification is expected, and south of it the more traditional westward intensification by Rossby waves takes place. Undercurrents are evident in the model results, but show a northward shift with respect to the surface currents. The reason for this shift is not clear but is probably associated with the interaction of these intermediate currents with the bottom topography.

[34] Although less important, the effects of the wind field are also evident in the results, especially at the southern part of the Red Sea where the winds have their greatest variability and become very strong during winter. The winds in the southern Red Sea affect strongly the exchange flow at the strait of Bab el Mandeb and through this the dynamical balances of the whole basin.

[35] Future observations and numerical simulations can hopefully produce a more accurate and complete picture of

the Red Sea circulation. The weakest point of all the attempts is our understanding of the air-sea fluxes in the area. Although recent observations enable us to put some constraints on the fluxes, our knowledge of the spatial and temporal variability of the forcing fields is very poor. The use of real fresh water fluxes rather than a virtual salt flux is another important improvement for future modeling attempts. The addition or subtraction of fresh water from the surface of the sea may play a role in the general dynamics of the area, and give rise to additional Goldsbrough-Stommel type circulation elements [Goldsbrough, 1933; Stommel, 1957, 1984].

[36] The only direct observations of the circulation in the area of the RSOW formation shown by the model come from a series of drifter tracks [Clifford *et al.*, 1997] during different seasons and years. All drifter tracks show a cyclonic rotation and, although the number is small (5), they favorably support the results presented here. So, the scenario proposed in this paper is that a large proportion (about 65%) of the hypersaline outflow exiting the strait of Bab el Mandeb is produced in a cyclonic gyre at the northern end of the Red Sea. This is twice the rate of RSOW formation proposed by Cember [1988]. It is important to note that the results presented here are from a model which is forced by climatological (monthly mean) conditions of the Red Sea. In most of the explored cases of open ocean deep or intermediate water formation, the associated processes take place on shorter timescales, during events of especially strong atmospheric forcing [Leaman and Schott, 1991]. The investigation of the effect of the variability of the atmospheric forcing at frequencies higher than the seasonal (synoptic timescales) is very important for our understanding of this kind of process. Thus, a logical next step is to perform numerical experiments including synoptic atmospheric forcing.

[37] More observations are needed in the Red Sea to determine the spatial structure and seasonality of the general circulation and to test the results of model simulations. Apart from a few known features (e.g., the cyclonic gyre in the north) and the well-documented exchange at Bab el Mandeb, many features of the circulation remain obscure. Especially near the boundaries, there are few observations, and these will be essential to determine whether the boundary currents and gyres predicted by these simulations exist.

[38] **Acknowledgments.** This work is supported by Office of Naval Research contract N00014-95-1-0025.

## References

- Alverson, K., and W. B. Owens, Topographic preconditioning of open-ocean deep convection, *J. Phys. Oceanogr.*, **26**, 2196–2213, 1996.
- Bleck, R., and E. P. Chassignet, Simulating the oceanic circulation with isopycnic-coordinate models, in *The Oceans: Physical-Chemical Dynamics and Human Impact*, edited by S. K. Majumdar *et al.*, pp. 17–39, Penn. Acad. of Sci., Philadelphia, 1994.
- Bleck, R., C. Rooth, D. Hu, and L. T. Smith, Salinity-driven thermocline transients in wind- and thermohaline-forced isopycnic coordinate model of the North Atlantic, *J. Phys. Oceanogr.*, **22**, 1486–1505, 1992.
- Cember, R. P., On the sources, formation, and circulation of Red Sea Deep Water, *J. Geophys. Res.*, **93**, 8175–8191, 1988.
- Clarke, R. A., and J. C. Gascard, The formation of Labrador Sea Water, I, Large-scale processes, *J. Phys. Oceanogr.*, **13**, 1764–1778, 1983.
- Clifford, M., C. Horton, J. Schmitz, and L. H. Kantha, An oceanographic nowcast/forecast system for the Red Sea, *J. Geophys. Res.*, **102**, 25,101–25,122, 1997.
- da Silva, A. M., C. C. Young, and S. Levitus, Atlas of Surface Marine Data 1994, vol. 1, Algorithms and Procedures, *NOAA Atlas NESDIS 8*, 83 pp., Natl. Oceanic and Atmos. Admin., Washington, D. C., 1994.
- Goldsbrough, G., Ocean currents produced by evaporation and precipitation, *Proc. R. Soc. London, Ser. A*, **141**, 512–517, 1933.
- Gordon, A. L., Deep Antarctic convection west of Maud Rise, *J. Phys. Oceanogr.*, **8**, 600–612, 1978.
- Hogg, N. G., The preconditioning phase of Medoc 1969, II, Topographic effects, *Deep Sea Res.*, **20**, 449–459, 1973.
- Koninklijk Nederlands Meteorologisch Instituut, Red Sea and Gulf of Aden oceanographic and meteorological data, *Publ. 129*, 26 pp., de Bilt, Netherlands, 1949.
- Lascaratos, A., Estimation of deep and intermediate water mass formation rates in the Mediterranean Sea, *Deep sea Res.*, **40**, 1327–1332, 1993.
- Lascaratos, A., R. G. Williams, and E. Tragou, A mixed-layer study of the formation of Levantine Intermediate Water, *J. Geophys. Res.*, **98**, 14,739–14,749, 1993.
- Leaman, K. D., and F. A. Schott, Hydrographic structure of the convection regime in the Gulf of Lions: Winter 1987, *J. Phys. Oceanogr.*, **21**, 575–598, 1991.
- Levitus, S., *Climatological Atlas of the World Ocean*, NOAA Prof. Pap. 13, 173 pp., U. S. Govt. Print. Off., Washington, D. C., 1982.
- Luksch, J., Expedition S. M. POLA in das Rota Meer, nordliche Halfte (October 1895–Mai 1896): Wissenschaftliche Ergebnisse, physikalische Untersuchungen, *Denkschrift d. kaiserl. Akad. Wissensch. in Wien* **69**, 337 pp., Vienna, 1901.
- Maillard, C., Eaux intermediaires et formation d'eau profonde en Mer Rouge, in *L'oceanographie physique de la Mer Rouge*, pp. 105–133, Cent. Natl. pour l'Exploitation des Oceans, Paris, 1974.
- Maillard, C., and G. Soliman, Hydrography of the Red Sea and exchanges with the Indian Ocean in summer, *Oceanol. Acta*, **9**, 249–269, 1984.
- Maury, M. F., *The Physical Geography of the Sea and its Meteorology*, 432 pp., Harvard Libr., Cambridge, Mass., 1855.
- McCreary, J. P., S. R. Shetye, and P. K. Kundu, Thermohaline forcing of eastern boundary currents: With application to the circulation off the west coast of Australia, *J. Mar. Res.*, **44**, 71–92, 1986.
- Morcos, S. A., Physical and chemical oceanography of the Red Sea, *Oceanogr. Mar. Biol. Ann. Rev.*, **8**, 73–202, 1970.
- Morcos, S., and G. F. Soliman, Circulation and deep water formation in the Northern Red Sea in winter (based on R/V Mabahis sections, January–February, 1935), in *L'oceanographie physique de la Mer Rouge*, pp. 91–103, Cent. Natl. pour l'Exploitation des Oceans, Paris, 1974.
- Muench, R. D., Relict convective features in the Weddell Sea, in *Deep Convection and Deep Water Formation in the Oceans*, edited by P. C. Chu and J. C. Gascard, pp. 53–67, Elsevier Sci., New York, 1988.
- Murray, S. P., and W. Johns, Direct observations of seasonal exchange through the Bab el Mandeb strait, *Geophys. Res. Lett.*, **24**, 2557–2560, 1997.
- Neumann, J., Evaporation from the Red Sea, *Isr. Explor. J.*, **2**, 153–162, 1952.
- Neumann, A. C., and D. A. McGill, Circulation of the Red Sea in early summer, *Deep Sea Res.*, **8**, 223–235, 1962.
- Patzert, W. C., Wind-induced reversal in Red Sea circulation, *Deep Sea Res.*, **21**, 109–121, 1974a.
- Patzert, W. C., Volume and heat transports between the Red Sea and Gulf of Aden, notes on the Red Sea heat budget, in *L'oceanographie physique de la Mer Rouge*, pp. 191–201, Cent. Natl. pour l'Exploitation des Oceans, Paris, 1974b.
- Pedgley, D. E., An outline of the weather and climate of the Red Sea, in *L'Oceanographie Physique de la Mer Rouge*, pp. 9–27, Cent. Natl. pour l'Exploitation des Oceans, Paris, 1974.
- Phillips, O. M., On turbulent convection currents and the circulation of the Red Sea, *Deep Sea Res.*, **13**, 1149–1160, 1966.
- Privett, D. W., Monthly charts of evaporation from the Indian Ocean (including the Red Sea and the Persian Gulf), *Q. J. R. Meteorol. Soc.*, **85**, 424–428, 1959.
- Quadfasel, D., and H. Baunder, Gyre-scale circulation cells in the Red Sea, *Oceanol. Acta*, **16**, 221–229, 1993.
- Schott, F., M. Visbeck, and J. Fischer, Observations of vertical currents and convection in the central Greenland Sea during the winter of 1988–1989, *J. Geophys. Res.*, **98**, 14,401–14,421, 1993.
- Siedler, G., Schichtungs- und Bewegungsverhältnisse am Sudausgang des Roten Meeres, *Meteor. Forschungsber.*, **A(4)**, 1–76, 1968.
- Siedler, G., General circulation of the water masses in the Red Sea, in *Hot Brines and Recent Heavy Metal Deposits in the Red Sea*, edited by E. T. Degens and D. A. Ross, pp. 131–137, New York, 1969.
- Sofianos, S. S., Circulation and water mass formation in the Red Sea, and the exchange with the Indian Ocean, Ph.D. thesis., Univ. of Miami, Miami, FL, 2000.

- Sofianos, S. S., and W. E. Johns, Wind induced sea level variability in the Red Sea, *Geophys. Res. Lett.*, *28*, 3175–3178, 2001.
- Sofianos, S. S., and W. E. Johns, An Oceanic General Circulation Model (OGCM) investigation of the Red Sea circulation, 1, Exchange between the Red Sea and the Indian Ocean, *J. Geophys. Res.*, *107*, 3196, doi:10.1029/2001JC001184, 2002.
- Sofianos, S. S., W. E. Johns, and S. P. Murray, Heat and freshwater budgets in the Red Sea from direct observations at Bab el Mandeb, *Deep Sea Res., Part II*, *49*, 1323–1340, 2002.
- Stommel, H., A survey of ocean current theory, *Deep Sea Res.*, *4*, 149–184, 1957.
- Stommel, H., The delicate interplay between wind-stress and buoyancy input in ocean circulation: The Goldsborough variations, *Tellus*, *36*, 111–119, 1984.
- Swallow, J. C., and G. F. Caston, The preconditioning phase of MEDOC 1969, I, Observations, *Deep Sea Res.*, *20*, 429–448, 1973.
- Thompson, E. F., Chemical and physical investigations: The general hydrography of the Red Sea, *John Murray Exped. 1933–34 Sci. Rep. 2*, pp. 83–103, Nat. Hist. Museum, London, 1939a.
- Thompson, E. F., Chemical and physical investigations. The exchange of water between the Red Sea and the Gulf of Aden over the “Sill”, *John Murray Exped. 1933–34 Sci. Rep. 2*, pp. 105–119, Nat. Hist. Museum, London, 1939b.
- Tragou, E., and C. Garrett, The shallow thermohaline circulation of the Red Sea, *Deep Sea Res., Part I*, *44*, 1355–1376, 1997.
- Tragou, E., C. Garrett, R. Outerbridge, and G. Gilman, The heat and freshwater budgets of the Red Sea, *J. Phys. Oceanogr.*, *29*, 2504–2522, 1999.
- Vercelli, E., Ricerche di oceanografia fisica eseguite della R. N. AMMIRAGLIO MAGNAGHI (1923–24), IV, La temperatura e la salinita, *Ann. Idrograf.*, *11*, 1–66, 1927.
- Vercelli, E., Nuove ricerche sulli correnti marine nel Mar Rosso, *Ann. Idrograf.*, *12*, 1–74, 1931.
- Visbeck, M., J. Fischer, and F. Schott, Preconditioning the Greenland Sea for deep convection: Ice formation and ice drift, *J. Geophys. Res.*, *100*, 18,489–18,502, 1995.
- Woelk, S., and D. Quadfasel, Renewal of deep water in the Red Sea during 1982–1987, *J. Geophys. Res.*, *101*, 18,155–18,165, 1996.
- Wyrki, K., On the deep circulation of the Red Sea, in *L’oceanographie physique de la Mer Rouge*, pp. 135–163, Cent. Natl. pour l’Exploitation des Oceans, Paris, 1974.
- Yegorov, N. I., Calculation of the heat balance of the Red Sea, *Meteorol. Igidrol.*, *3*, 49–56, 1950.

---

W. E. Johns, Rosenstiel School of Marine and Atmospheric Science, University of Miami, 4600 Rickenbacker Causeway, Miami, FL 33149, USA. (wjohns@rsmas.miami.edu)

S. Sofianos, Department of Physics, University of Athens, University Campus Building PHYS-5, Athens GR-15784, Greece. (sofianos@oc.phys.uoa.gr)